Supporting Information for

Sorption of Perfluoroalkyl Acids to Fresh and Aged Nanoscale Zerovalent Iron Particles

Yanyan Zhang, Yue Zhi, Jinxia Liu, Subhasis Ghoshal*

Department of Civil Engineering, McGill University, Montreal, Quebec H3A 0C3, Canada

Phone: (1)-514-398-6867; fax: (1)-514-398-7361; e-mail: subhasis.ghoshal@mcgill.ca

There are 20 pages, including 8 tables and 15 figures.

Contents:

This supporting information contains 20 pages, including 8 tables and 15 figures:

Figure S8. (A) Effect of ionic strength on the distribution ratio (log K_d) of PFOS to nZVI; (B) The zeta potential (ZP) of nZVI suspensions (0.1 g/L) at different ionic strength. Reduction in K_d that are statistically significant ($p < 0.05$) compared with zero ionic strength are marked with "*". The initial concentration of PFOS was 2000 μg/L and the average pH was 8.3. Mean and standard deviation of triplicates are shown.

Figure S9. (A) Sorption isotherm of humic acid (HA) to 0.1 g/L nZVI (pH 8.7–9.5). The Freundlich sorption coefficient (log K_F), nonlinearity index (n), and coefficient of determination (R^2) are shown. Solid line is drawn to guide the eye. (B) Zeta potential (ZP) of nZVI (0.1 g/L) at different initial concentrations of HA (pH 9.2–9.5) in 5 mM NaCl solution. Mean and standard deviations of triplicates are shown.

Figure S10. TEM image for (A) nZVI particles aging in deoxygenated water for 20 days (nZVI-20 d); (B) nZVI particles aging in deoxygenated water for 60 days (nZVI-60 d); (C) synthesized $Fe(OH)_2$. The particles were dispersed in water at 0.1 g/L.

Figure S11. Image for (A) fresh nZVI, (B) nZVI aging in deoxygenated water for 20 days (nZVI-20 d), (C) nZVI aging in deoxygenated water for 40 days (nZVI-40 d).

Figure S12. TEM image and EDS spectra recorded from the spot marked with "*" for (A) S-nZVI; (B) synthesized FeS; and (C) S-nZVI contacted in deoxygenated water for 20 days (S-nZVI-20 d). The particles were dispersed in water at 0.1 g/L.

Figure S13. TEM images for (A) aerobically aged nZVI (O-nZVI-72 h); (B) synthesized γ-Fe_2O_3; (C) synthesized Fe_3O_4; and (D) synthesized γ-FeOOH. The particles were dispersed in water at 0.1 g/L.

Figure S14. X-ray powder diffraction (XRD) spectra of the (A) aerobically aged nZVI (O-nZVI-72 h); and synthesized (B) Fe_3O_4, (C) γ-Fe_2O_3, and (D) γ-FeOOH compared with standard spectra (red line). The XRD analysis was conducted in ambient air with Cu Kα using a D8 Advance (Bruker) operated at 40 kV and 40 mA. Continuous scans from 10° to 90° at 2θ were collected with a stop size of 0.02° and a count time of 1.0 s per step.

Figure S15. ART-FTIR spectra of PFOS, synthesized iron nanoparticles that represent the iron species formed after aging, and PFOS sorbed on the iron nanoparticles for (A) $Fe(OH)_2$, (B) FeS, (C) γ-Fe_2O_3, (D) Fe_3O_4, and (E) γ-FeOOH. PFOS (500 mg/L) was incubated with 2.0 g/L particles for 5 days before analysis. The peak wavenumbers for characteristic functional groups of PFOS (C–F, R–SO_3^-) are shown.

SI-1. Target Compounds

Table S1. Formula, molecular weight, octanol-water partition coefficient (K_{ow}), and acid dissociation constant (pK_a) of the PFAAs used.

	Formula	Molecular weight, g/mol	Log K_{ow}[a], log (L/L)	pK_a
PFOS	$C_8F_{17}SO_3K$	538.22	5.25	–3.27[b]
PFHxS	$C_6F_{13}SO_3K$	399.11	--	--
PFDA	$C_9F_{19}COOH$	514.08	5.30	–0.2[c]
PFNA	$C_8F_{17}COOH$	464.08	4.84	–0.1[c]
PFOA	$C_7F_{15}COOH$	414.07	4.30	–0.2[c]

a. Predicted from COSMOtherm, which performs density functional quantum chemical continuum solvation calculations with statistical thermodynamics.[S1]
b. Calculated value obtained from the ACD/I-Lab Web Service.[S2]
c. Predicted from Gaussian09.[S3]

SI-2. Synthesized Methods for Aging Products of nZVI

Iron(II)hydroxide ($Fe(OH)_2$) particles were synthesized inside the chamber by slowly adding NaOH (1.6 g in 100 mL H_2O) to a continuously mixed solution of $FeSO_4 \cdot 7H_2O$ (11.2 g in 200 mL H2O), followed by stirring for 24 h.[S4] The suspension was centrifuged and the particles were washed one time with H_2O and one time with methanol, then dried and stored inside the chamber.

Mackinawite (FeS) particles were prepared inside the chamber by adding 0.3 M $Na_2S \cdot 9H_2O$ (100 mL) solution dropwise to a continuously mixed solution of 0.3 M $FeCl_2 \cdot 4H_2O$ (100 mL),[S5] followed by stirring for five days. The suspension was centrifuged and the particles were washed three times with water and two times with methanol, then dried and stored inside the chamber.

Magnetite (Fe_3O_4) particles were prepared inside the chamber by precipitating a continuously mixed solution of $FeCl_3 \cdot 6H_2O$ and $FeCl_2 \cdot 4H_2O$ (10.4 g and 4.0 g in 200 mL of water) at pH ~8.0.[S6] Ammonium hydroxide was added dropwise to raise the pH where the solution turned from brown to black and the stirring continued for another 10 min. The black particles were then magnetically separated, washed three times with water and three times with methanol, dried, and stored inside the chamber.

Maghemite (γ-Fe_2O_3) particles were prepared by oxidizing the synthesized Fe_3O_4 at 250 °C under an air atmosphere for 2 h.[S7]

Lepidocrocite (γ-FeOOH) particles were prepared by oxidizing a continuously mixed solution of $FeSO_4 \cdot 7H_2O$ (16.68g in 300 mL of water) at pH 6.7–6.9 (raise pH by adding 1 M NaOH) with constant air supply.[S7] The color of the precipitate changed from dark greenish blue to grey and finally to orange after ~2 h. The orange particles were washed five times with water and dried at 80 °C.

SI-3. Aqueous Concentration Change over Time

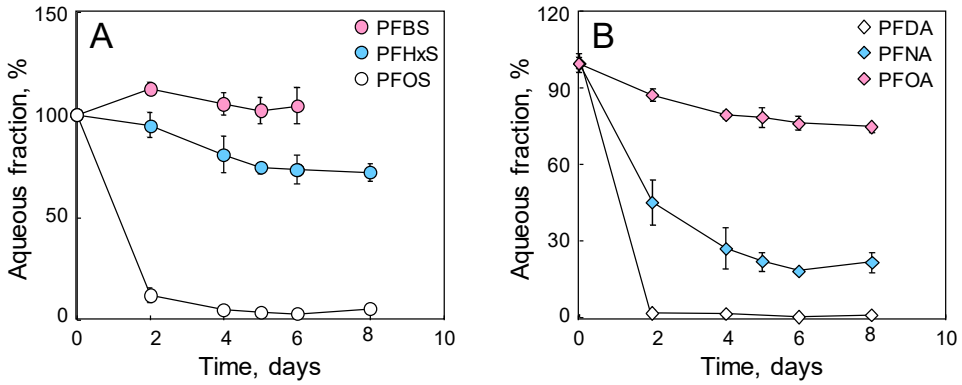

Figure S1. Aqueous concentration change over time for (A) sorption of 10 mg/L of PFOS to 0.4 g/L of nZVI, and 20 mg/L PFHxS and PFBS to 1.2 g/L nZVI; (B) sorption of 20 mg/L PFDA, 10 mg/L of PFNA, and 10 mg/L PFOA to 0.4 g/L of nZVI. Mean and standard deviation of triplicates are shown.

SI-4. Effect of Solution Chemistry

Effect of pH. The pH of the suspension was adjusted by adding 0.1 M HCl or 0.1 M NaOH before the sorption experiment and the final pH after the sorption experiment was measured as the test pH.

Effect of ionic strength. The ionic strength of the suspension was adjusted by adding NaCl or $CaCl_2$ solution.

Effect of occurrence of HA (without washing). The nZVI suspension (0.1 g/L) was incubated with PFOS (2000 µg/L) in the presence of HA (5–200 mg/L) for 5 days. After centrifugation (4500 rpm, 20 min), PFOS concentration in the aqueous and solid phase was extracted and measured, respectively.

Effect of loading CMC and HA (with washing). The nZVI suspension (0.1 g/L) was incubated with CMC (20–400 mg/L) or HA (5–200 mg/L) for 24 h. The time period was enough to reach sorption equilibrium for both CMC and HA. The nZVI was magnetically precipitated and the supernatant was removed completely for TOC analysis. Then PFOS at 2000 µg/L was added in 5 mM NaCl solution and the sorption continued for 5 days. After centrifugation (4500 rpm, 20 min), PFOS concentration in the aqueous and solid phase was extracted and measured, respectively. TOC in the aqueous phase was also measured and there was no detectable value, indicating that there were no CMC or HA remaining in the aqueous phase. Sorption of HA and CMC to nZVI was fitted to Freundlich equation.

SI-5. Extraction and Analytical Methods of PFAAs

Extraction method. The PFAA concentration in the aqueous phase was determined by sampling an aliquot of 400 µL from the aqueous phase after sorption experiment inside the chamber, followed by centrifugation at 16 000 rpm for 10 min and dilution with acetonitrile. The remaining solution was centrifuged at 4500 rpm for 20 min. The supernatant was decanted and the PFAA in the solid phase was extracted by sonicating in 15 mL of acetonitrile/250 mM NaOH (9/1,v/v) for 30 min, followed by shaking at 175 rpm for 30 min. The extract was

neutralized by adding 250 mM HCl and then diluted with acetonitrile. The extract after dilution was spiked with internal standards before quantification analysis.

Dissolved Fe was reported to form aqueous-phase complexes with PFAAs and reduce the quantifiable levels.[S8] In the current study, the concentration of dissolved Fe (mostly Fe^{2+}) was ≤ 7.4 mg/L in the aqueous phase after sorption experiments. In the preliminary test, over 90% of PFOS in 10 mg/L of Fe^{2+} solution and over 94% of PFOA in 100 mg/L Fe^{2+} solution were quantified, respectively, indicating that the Fe^{2+} level in the current study does not significantly affect the quantifiable concentrations of PFAAs through complexation.[S8]

Table S2. Spike recoveries of PFAAs sorbed to nZVI by solvent extraction with acetonitrile/250 mM NaOH (9/1, v/v). Mean and standard deviation of triplicates are shown.

Recovery	PFOS	PFHxS	PFBS	PFDA	PFNA	PFOA
Mean	99.4%	99.6%	96.8%	99.2%	99.5%	99.8%
Standard deviation	0.25%	0.16%	3.5%	0.28%	0.22%	0.20%

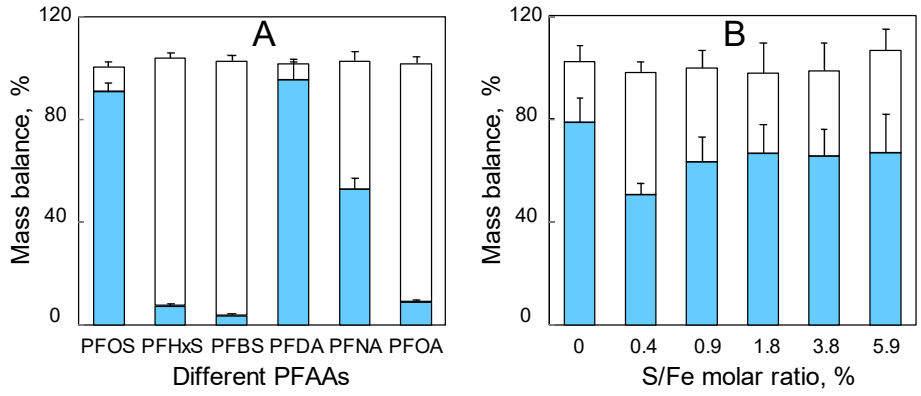

Figure S2. Mass balance for (A) sorption of PFOS, PFHxS, PFBS, PFDA, PFNA, and PFOA to nZVI particles (initial concentration of 10 mg/L for the target compounds and 0.4 g/L of nZVI were used); (B) sorption of PFOS to S-nZVI particles with different S/Fe molar ratios (initial concentration of 10 mg/L of PFOS and 0.1 g /L of nZVI particles were used). The contributions from aqueous (white) and solid (blue) phase are shown separately. Mean and standard deviation of triplicates are shown.

Table S3. Quantitative analytical method of PFAAs.

Instrument	Shimadzu Nexera UHPLC coupled to an AB Sciex 5500 QTRAP mass spectrometer				
Ionization	Negative electrospray				
Acquisition mode	Multiple reaction monitoring (scheduled MRM)				
Analytical column	Ascentix Express F5, 2.7 µm, 100 × 2.1 mm				
Delay column	Kinetex EVO C18, 5 µm, 50 × 3.1 mm				
Column temperature	40 °C				
Injection volume	5 µL				
Mobile phases	A: 0.15% acetic acid in HPLC water; B: 0.15% acetic acid in acetonitrile				
Calibration	Linear calibration curve, 1/x weighted				
Gradient profile	Time (min)	Percentage B (%)	Flow rate (mL/min)		
	1.0	5	0.4		
	5.0	95	0.4		
	8.0	95	0.4		
	8.1	5	0.4		
	10	Stop			
Monitored ion transitions	Analytes	Ion transitions	Internal standards	Ion transitions	Calibration range (µg/L)
	PFOS	499.0 > 79.9	MPFOS	503.0 > 79.9	0.05–20
	PFHxS	399.2 > 79.9	MPFHxS	403.0 > 103.0	0.05–20
	PFBS	299.1 > 80.0	MPFHxS	403.0 > 103.0	0.05–20
	PFDA	513.0 > 469.0	MPFDA	515.0 > 470.0	0.05–20
	PFNA	463.0 > 419.0	MPFNA	468.0 > 423.0	0.05–20
	PFOA	413.0 > 369.0	MPFOA	417.0 > 372.0	0.05–20

SI-6. TEM of nZVI particles

Methods. TEM analysis of nZVI and other particle suspensions was performed using an FEI Tecnai G2 F20 S/TEM equipped with Gatan Ultrascan 4000 4k × 4k CCD Camera System (Model 895). An EDAX Octane T Ultra W/Apollo XL T2 SDD system was used for energy dispersive X-ray spectroscopy (EDS) measurements.

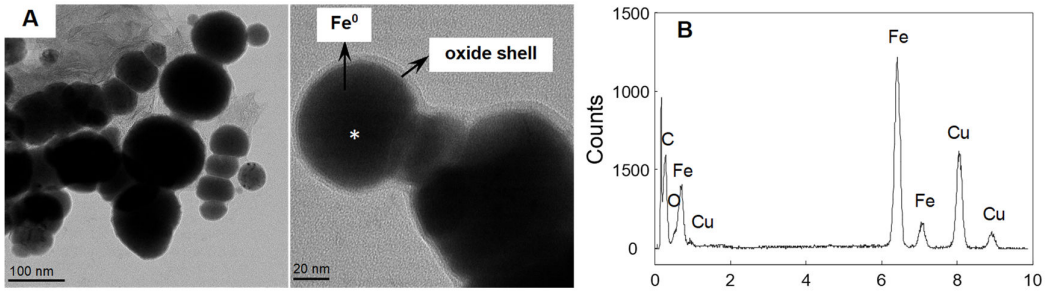

Figure S3. (A) TEM image of nZVI particles and (B) EDS spectrum recorded from the spot marked with "*". The particles were dispersed in water at 0.1 g/L.

SI-7. Mass Balance of Perfluorooctanoic Acid (PFOA) and Perfluorooctanesulfonic Acid (PFOS) Incubated with nZVI and Surface-Modified nZVI

Methods. PFOA (5 or 10 mg/L) and PFOS (5 or 10 mg/L) were incubated with 10 mL of 2.0 g/L nZVI or surface-modified nZVI suspensions in 22 mL or 160 mL (for heating up experiments) glass vials. The suspensions were prepared inside the chamber with deoxygenated water, and the vials were fitted with butyl rubber stoppers and crimp sealed and shaken at 175 rpm at 25 or 65 °C for 7 days. After incubation, the nZVI particles were precipitated by super magnet. The PFOA and PFOS in the aqueous phase was determined by sampling an aliquot of 100 µL from the supernatant and diluted with acetonitrile. Then the supernatant was decanted and the PFOA and PFOS in the solid phase was extracted by sonicating in 15 or 30 mL of acetonitrile/250 mM NaOH (9/1,v/v) for 30 min, followed by shaking at 175 rpm for 30 min. The extract was neutralized by adding 250 mM HCl and then diluted with acetonitrile. The extract after dilution was spiked with internal standards before quantification analysis. The mass balance of PFOA and PFOS after incubation with nZVI and surface-modified nZVI was referred to as the percentage of total concentration from the aqueous and solid phases relative to the value from the corresponding control tests. The results of the mass balance are shown in **Table S4**.

The degradation of nZVI on PFOA and PFOS was tested for bare nZVI and different surface-modified nZVI and amendments (**Table S4**), including sulfidated nZVI (S-nZVI) with a S/Fe molar ratio of 3.8% at 25 °C, nZVI particles accompanied by activated carbon (nZVI + AC) at a nZVI/AC mass ratio of 1:3 at 25 °C, nZVI particles accompanied by 0.22 mM Vitamin B12 at 25 °C (nZVI + Vitamin B12) and by 0.5 mM Vitamin B12 at 65 °C (nZVI + Vitamin B12 + 65 °C), Ni modified nZVI (Ni-nZVI) at a Ni/Fe molar ratio of 1:4 at 25 °C, Ni-nZVI particles accompanied by activated carbon (Ni-nZVI + AC) at a Ni-nZVI/AC mass ratio of 1:3 at 25 °C, palladium doped nZVI at 25 °C (Pd-nZVI) and at 65 °C (Pd-nZVI + 65 °C), Pd-nZVI in the presence of butanol (Pd-nZVI + butanol) at a butanol/H_2O ratio of 9:1 (v/v) at 25 °C, and Pd-nZVI particles accompanied by 0.5 mM Vitamin B12 at 25 °C (Pd-nZVI + Vitamin B12) and by 0.5 mM Vitamin B12 at 65 °C (Pd-nZVI + Vitamin B12 + 65 °C).

Table S4. Mass balance for PFOA and PFOS incubated with NZVI and surface-modified NZVI particles. Mean and standard (STD) deviation of triplicates are shown.

	PFOA		PFOS[a]	
NZVI type and amendments	Mean	STD	Mean	STD
Bare NZVI	108%	6.5%	94.4%	4.9%
S-NZVI	91.6%	3.8%	98.9%	1.1%
NZVI + AC	103%	1.7%	114%	7.2%
NZVI + Vitamin B12	112%	4.3%	96.2%	3.3%
nZVI + Vitamin B12 + 65 °C	129%	3.0%	94.2%	4.7%
Ni-nZVI	108%	4.3%	116%	6.1%
Ni-nZVI +AC	106%	2.9%	112%	3.9%
Pd-nZVI	95.0%	4.6%	109%	15%
Pd-nZVI + 65 °C	124%	3.5%	115%	2.1%
Pd-nZVI + butanol	98.8%	3.6%	94.2%	0.6%
Pd-nZVI + Vitamin B12	105%	5.8%	84.3%	2.4%
Pd-nZVI + Vitamin B12 + 65 °C	118%	8.7%	105%	8.8%

a. Linear PFOS.

SI-8. ATR-FTIR Spectra

Methods. Before analysis, nZVI (2.0 g/L) was incubated with 500 mg/L PFOS, PFHxS, and PFNA solution in 22 mL glass vials, respectively. The suspensions were prepared inside the chamber with deoxygenated water, and the vials were fitted with butyl rubber stoppers, crimp sealed, and shaken at 175 rpm at 25 °C for 5 days. Right before ATR-FTIR analysis, the nZVI particles were precipitated with a magnet and the supernatant was decanted. The wet particles were applied to the diamond ATR crystal and the ATR-FTIR spectra were recorded immediately. The spectrum of the precipitated particles from nZVI suspension without PFAA was used as reference. The spectra of PFOS, PFHxS, and PFNA was obtained by applying solid suspension of the chemicals to the diamond ATR crystal.

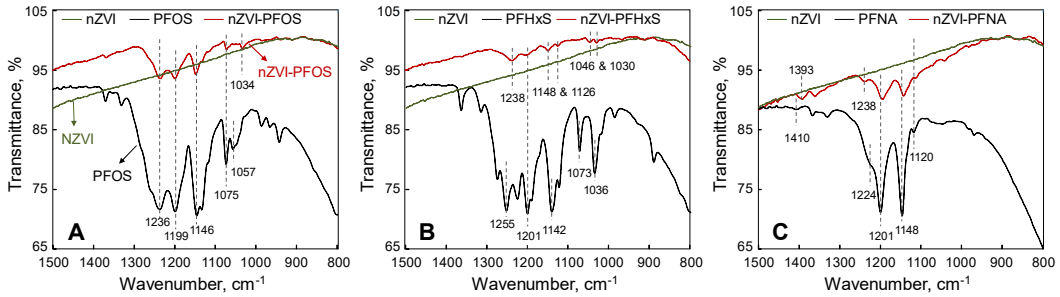

Figure S4. ATR–FTIR spectra of nZVI, PFAAs, and PFAAs sorbed on nZVI for (A) PFOS, (B) PFHxS, and (C) PFNA. The peak wavenumbers for characteristic functional groups of PFAAs (C–F, R–COO^-, R–SO_3^-) are shown.

Table S5. Position (wavenumber, cm^{-1}) and vibration (ν) mode assignments of major IR bands in ATR-FTIR spectra of PFOS, PFHxS, and PFNA, and those sorbed on nZVI (ν_{as}, asymmetric stretch; ν_s, symmetric stretch).

Wavenumber, cm^{-1}		Vibration mode assignment	Change in spectrum
PFOS	nZVI-PFOS		
1371	1369	ν (C–C)	
1332		ν (C–C)	
1260		ν (C–C)	
1236	1236	ν_{as} (C–F) + ν_{as} (R–SO_3^-)	
1199	1199	ν_{as} (CF_2)	
1146, 1134	1148	ν_s (C–F) + ν (C–C)	peak shape
1075	1073	ν (C–C) + ν_s (C–F) + ν_s (R–SO_3^-)	
1057	1034	ν_s (R–SO_3^-)) + ν (C–C)	shifting to lower wavenumber
PFHxS	nZVI-PFHxS		
1365		ν (C–C)	
1316		ν (C–C)	
1277		ν (C–C)	
1255	1238	ν_{as} (C–F) + ν_{as} (R–SO_3^-)	shifting to lower wavenumber

1226		ν_{as} (C–F) + ν_{as} (R–SO_3^-)	peak shape
1201, 1191	1206	ν_{as} (CF_2)	
1142	1148	ν_s (C–F) + ν (C–C)	
1124	1126		
1073	1046	ν (C–C) + ν_s (C–F) + ν_s (R–SO_3^-)	shifting to lower wavenumber
1036	1030	ν_s (R–SO_3^-)$^-$) + ν (C–C)	shifting to lower wavenumber
PFNA	nZVI-PFNA		
1410	1393	ν_s (R–COO^-) + ν (C–C)	shifting to lower wavenumber
1369	1363	ν (C–C)	
1332		ν (C–C)	
1224	1238	ν_{as} (C–F)	shifting
1201	1195	ν_{as} (C–F)	shifting
1148	1144	ν_s (C–F) + ν (C–C)	
1120	1116	ν_s (C–F) + ν (C–C)	

SI-9. Free Energy Associated with Sorption

The change in free energy associated with the sorption of PFOS ($\Delta G_{sorption}$, kJ/mol) to nZVI was considered to comprise a hydrophobic ($\Delta G_{hydrophobic}$, kJ/mol) and an electrostatic ($\Delta G_{electrostatic}$, kJ/mol) part (only sorbate-sorbent interaction is considered):[S9]

$$\Delta G_{sorption} = -RT \ln K_d = \Delta G_{hydrophobic} + \Delta G_{electrostatic} = \Delta G_{hydrophobic} + z\psi F \qquad \text{(S1)}$$

where R (= 8.31 J/(mol·K)) is the gas constant; T (= 293.15 K) is the absolute temperature; z (= –1) is the number of charge for the exchanging ion; ψ (V or J/C) is the surface potential relative to the bulk solution, which can be approximated by zeta potential (ZP); F (= 96 485 C/mol) is the Faraday constant. $\Delta G_{sorption}$ of PFOS sorption to nZVI at C_w of 100 µg/L was calculated to be –26.3 kJ/mol using K_d (dimensionless K_d value was obtained by multiplying K_d in L/kg with the density of water, 1 kg/L).

The ZP of nZVI ranged from –0.9 to +17.8 mV in 5 mM NaCl solution with PFOS present at tested concentrations (**Figure S5**). In any case, the contribution from $\Delta G_{electrostatic}$ (–1.72 to +0.09 kJ/mol) to $\Delta G_{sorption}$ was not large. While $\Delta G_{hydrophobic}$ contributes at least 93.5% to $\Delta G_{sorption}$ at C_w of 100 µg/L, suggesting dominance of hydrophobic effect in the interactions between PFOS and nZVI under the test conditions. The electrostatic repulsion between PFOS molecules was not considered in the calculations, but it would only hinder the sorption thus making the hydrophobic effect more important.[S10]

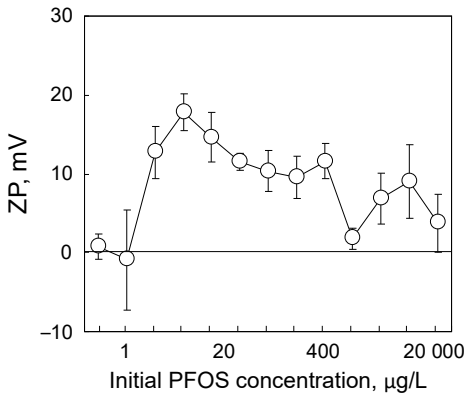

Figure S5. Zeta potential (ZP) of nZVI (0.1 g/L) in 5 mM NaCl with different initial concentrations of PFOS (0–20 000 µg/L). Mean and standard deviation of triplicates are shown.

SI-10. Sorption Data on Specific Surface Area Basis

Table S6. Freundlich regression parameters and the coefficient of determination (R^2) and concentration-specific distribution ratios ($K_{d,SA}$, L/m^2) on specific surface area basis for sorption of PFOS to nZVI, aged nZVI, and the synthesized iron nanopartilces that represent the iron species formed after aging.

			Freundlich fitting results			Concentration-specific log $K_{d,SA}$, log (L/m^2)			
Solid[a]	Surface area, m^2/g	pH/pH$_{pzc}$[b]	log $K_{F,SA}$[c]	N[c]	R^2	2.5 µg/L	20 µg/L	100 µg/L	1000 µg/L
nZVI	5.54	8.5/8.6	1.33 ± 0.04	0.85 ± 0.02	0.984	1.26	1.12	1.02	0.86
S-nZVI	10.44	9.4/8.6	0.02 ± 0.05	0.92 ± 0.02	0.979	-0.02	-0.09	-0.14	-0.22
$Fe(OH)_2$	5.42	8.0/8.6	0.79 ± 0.04	0.91 ± 0.02	0.983	0.75	0.68	0.62	0.53
FeS	35.8	6.9/-	-1.56 ± 0.07	0.81 ± 0.04	0.925	-1.64	-1.81	-1.95	-2.14
O-NZV-72 h	62.8	8.6/8.7	-0.11 ± 0.03	0.72 ± 0.01	0.987	-0.22	-0.47	-0.67	-0.95
γ-Fe_2O_3[d]	76.9	4.8/3.2	-0.31 ± 0.05	0.68 ± 0.03	0.967	-0.44	-0.72	-0.94	--
Fe_3O_4[d]	82	6.9/6.9	-0.21 ± 0.06	0.79 ± 0.05	0.937	-0.30	-0.49	-0.63	--
γ-FeOOH[d]	82.7	7.4/8.0	-0.12 ± 0.05	0.81 ± 0.04	0.961	-0.20	-0.37	-0.50	--

a. The solid concentration used in the sorption tests was 0.1 g/L.

b. pH$_{pzc}$ is the point of zero charge measured in 5 mM NaCl.

c. The unit of the Freundlich sorption coefficient ($K_{F,SA}$) is (µg/m^2)/(µg/L)^n; standard errors of log $K_{F,SA}$ and n are shown

d. Only C_w in the range of 1–500 µg/L was used for the regression.

SI-11. Sorption Data in the Literature

Table S7. Sorption data of PFOS to minerals, sediments, and soils in the literature.

Minerals	Isotherm	Initial range	Log K_d	pH	pH_{zpc}	BET, m^2/g	Reference
Kaolinite ($Al_2Si_2O_5(OH)_4$)	Langmuir/linear	120–8000 μg/L	0.73	--	pH 4.6	10.0	(S11)
Kaolinite	Linear	100–3000 μg/L	1.16	7.5	pH 5.1	10.0	(S10)
Goethite (α-FeOOH)	Langmuir/linear	120–8000 μg/L	0.90	--	pH 7.5–9.5	58.0	(S11)
Geothite	Langmuir	5–1000 μg/L	2.69–3.08	7.0	pH 9.4	76.1	(S12)
Nano Fe_2O_3	Linear	50–1000 μg/L	3.38	7.0	pH 7.6	41.7	(S13)
Boehmite (γ-AlO(OH))	Langmuir/Freundlich	50–1000 μg/L	2.85–3.17	7.0	pH 8.4	299.2	(S14)
Alumina (Al_2O_3)	Langmuir/Freundlich	40–400 μg/L	2.42–2.80	7.0	pH 8.5	88.6	(S15)
Sediments	**Isotherm**	**Initial range**	**Log K_F**	**pH**	***n***	**BET, m^2/g**	**Reference**
Sediment 1	Freundlich	0.5–100 μg/L	1.43	7.0	0.95	18.0	(S16)
Sediment 2	Freundlich	0.5–100 μg/L	0.78	7.5	0.86	27.0	(S16)
Sediment 3	Freundlich	0.5–100 μg/L	1.29	7.6	0.96	27.0	(S16)
Sediment 5	Freundlich	0.5–100 μg/L	2.35	5.7	0.81	8.0	(S16)
Miyun Sediment	Freundlich	500–5000 μg/L	1.75	7.0	0.69	21.3	(S17)
Soils	**Isotherm**	**Initial range**	**Log K_F**	**pH**	***n***	**f_{OC}, %**	**Reference**
Sandy Clay Loam	Freundlich	0.5–1000 μg/L	0.55	6.5	0.94	0.8	(S18)
Loamy Sand	Freundlich	0.5–1000 μg/L	0.36	6.5	0.88	1.7	(S18)
Loam	Freundlich	0.5–1000 μg/L	1.11	6.5	0.83	4.5	(S18)

SI-12. Effect of CMC

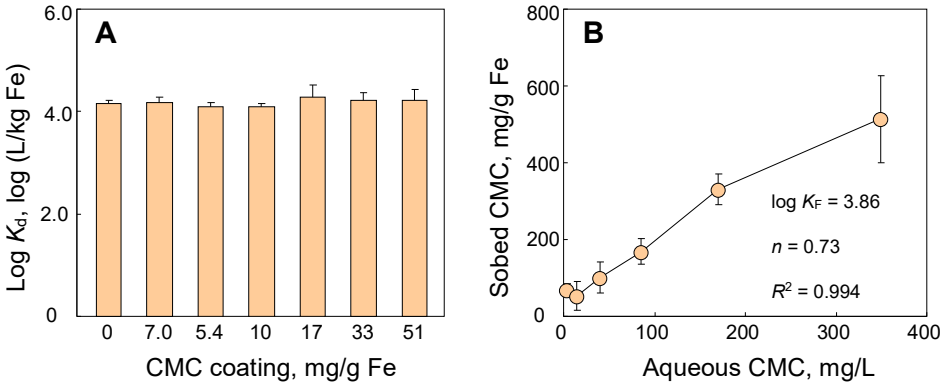

Figure S6. (A) Effect of carboxymethyl cellulose (CMC) coating on the distribution ratio (log K_d) of PFOS to nZVI. The initial concentration of PFOS was 2000 μg/L. (B) Sorption isotherm of CMC to 0.1 g/L nZVI (pH 8.3–8.7). The Freundlich sorption coefficient (K_F, (mg/kg Fe)/(mg/L)^n), nonlinearity index (n), and coefficient of determination (R^2) are shown. Solid line is drawn to guide the eye. Mean and standard deviations of triplicates are shown.

SI-13. Solution Chemistry

Table S8. Free energy associated with sorption ($\Delta G_{sorption}$, kJ/mol) and electrostatic interaction ($\Delta G_{electrostatic}$, kJ/mol) over pH change.

Sample pH	Zeta potential, mV	$\Delta G_{sorption}$, kJ/mol	$\Delta G_{electrostatic}$, kJ/mol
7.0	17.77	-27.2	-1.7
7.9	11.43	-25.2	-1.1
8.7	1.59	-24.4	-0.2
9.6	-4.01	-21.0	0.4
10.8	-34.53	-18.8	3.3

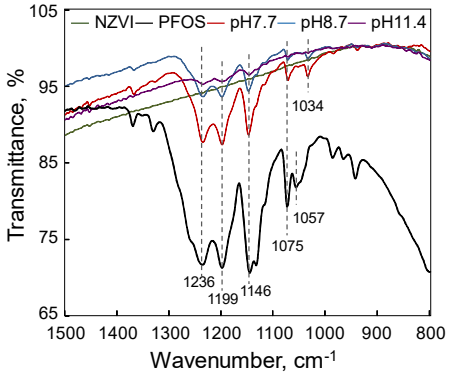

Figure S7. ART–FTIR spectra of nZVI, PFOS, and PFOS sorbed on nZVI at pH 7.7, pH 8.7, and pH 11.4. PFOS (500 mg/L) was incubated with 2.0 g/L nZVI for 5 days before analysis. The peak wavenumbers for characteristic functional groups of PFOS (C–F, R–SO_3^-) are shown.

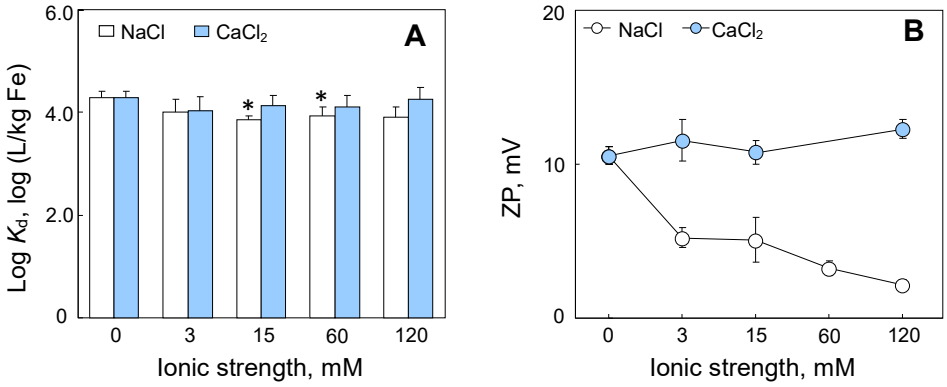

Figure S8. (A) Effect of ionic strength on the distribution ratio (log K_d) of PFOS to nZVI; (B) The zeta potential (ZP) of nZVI suspensions (0.1 g/L) at different ionic strength. Reduction in K_d that are statistically significant ($p < 0.05$) compared with zero ionic strength are marked with "*". The initial concentration of PFOS was 2000 μg/L and the average pH was 8.3. Mean and standard deviation of triplicates are shown.

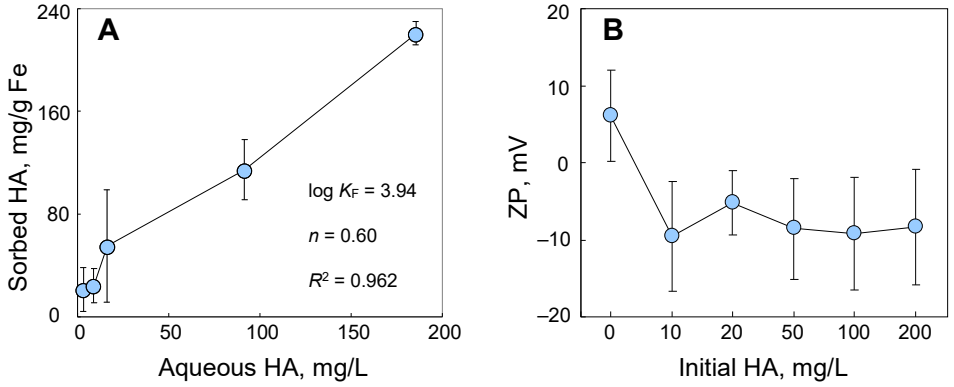

Figure S9. (A) Sorption isotherm of humic acid (HA) to 0.1 g/L nZVI (pH 8.7–9.5). The Freundlich sorption coefficient (K_F, (mg/kg Fe)/(mg/L)^n), nonlinearity index (n), and coefficient of determination (R^2) are shown. Solid line is drawn to guide the eye. (B) Zeta potential (ZP) of nZVI (0.1 g/L) at different initial concentrations of HA (pH 9.2–9.5) in 5 mM NaCl solution. Mean and standard deviations of triplicates are shown.

SI-14. Anaerobic Aging and Sulfidation

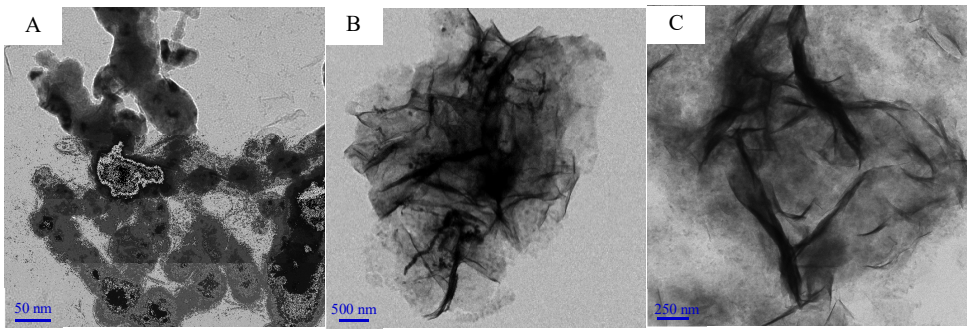

Figure S10. TEM image for (A) nZVI particles aging in deoxygenated water for 20 days (nZVI-20 d); (B) nZVI particles aging in deoxygenated water for 60 days (nZVI-60 d); (C) synthesized $Fe(OH)_2$. The particles were dispersed in water at 0.1 g/L.

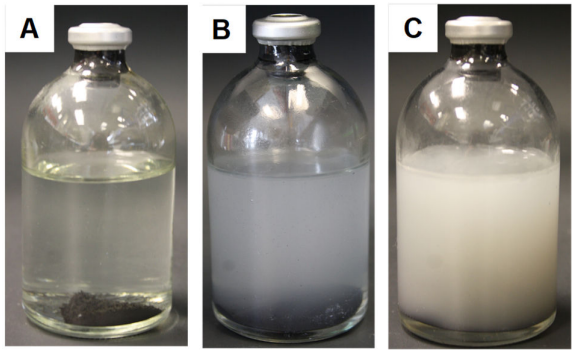

Figure S11. Image for (A) fresh nZVI, (B) nZVI aging in deoxygenated water for 20 days (nZVI-20 d), (C) nZVI aging in deoxygenated water for 40 days (nZVI-40 d).

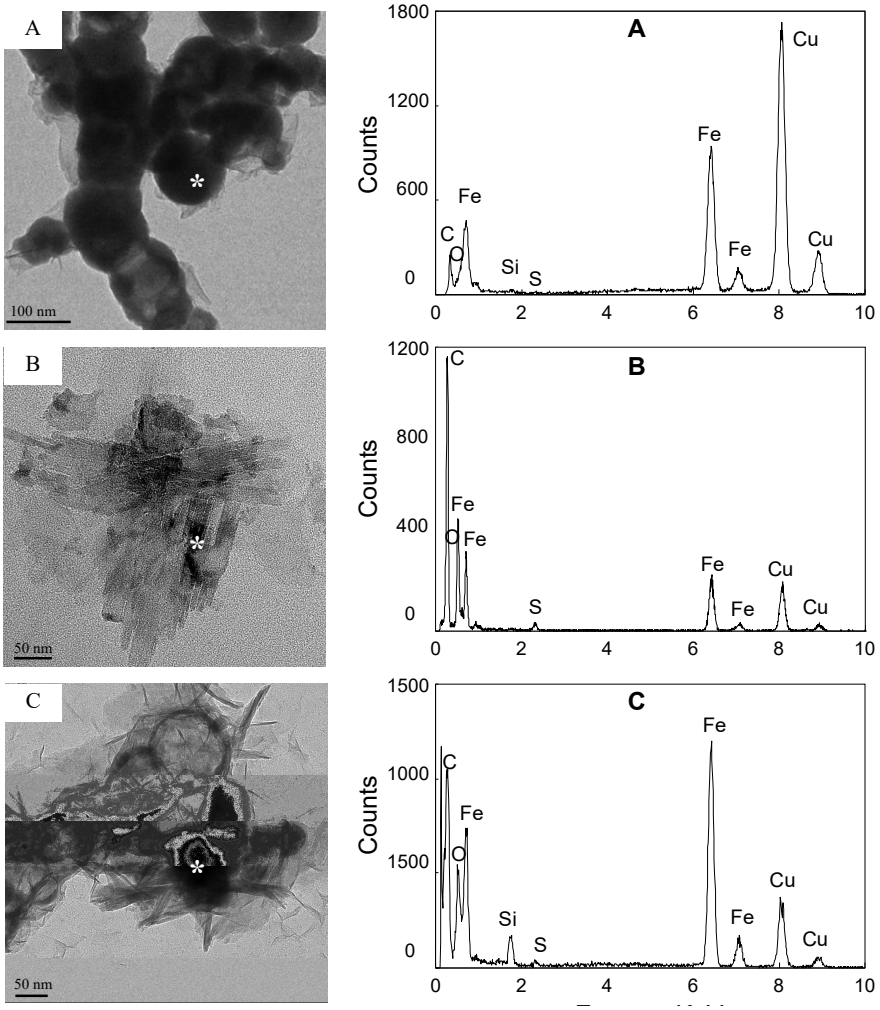

Figure S12. TEM image and EDS spectra recorded from the spot marked with "*" for (A) S-nZVI; (B) synthesized FeS; and (C) S-nZVI contacted in deoxygenated water for 20 days (S-nZVI-20 d). The particles were dispersed in water at 0.1 g/L.

Results. S-nZVI particles had similar size and morphology with nZVI. FeS (5 mg/L) was a thin sheet with a width of ~30 nm and length of ~300. S-nZVI-20 d showed sheet-like structures outgrowing from the particle, which are characteristic of $Fe(OH)_2$.

S15. Aerobic Aging

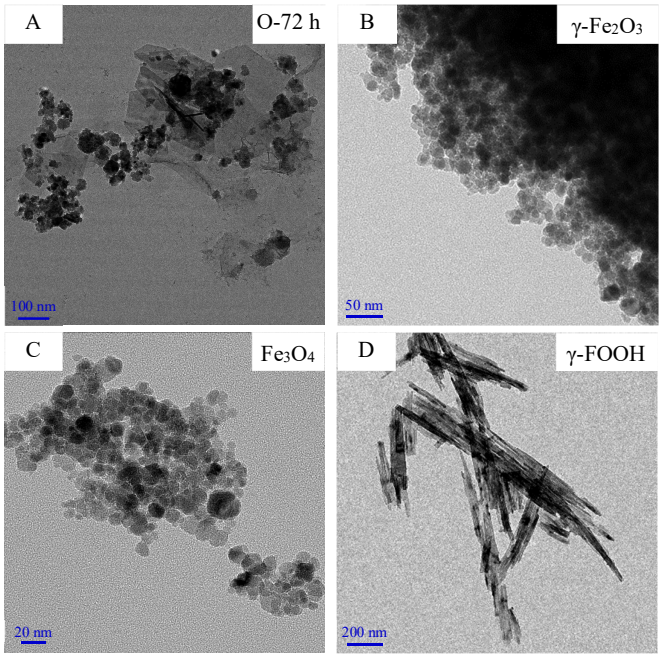

Figure S13. TEM images for (A) aerobically aged nZVI (O-nZVI-72 h); (B) synthesized γ-Fe_2O_3; (C) synthesized Fe_3O_4; and (D) synthesized γ-FeOOH. The particles were dispersed in water at 0.1 g/L.

Results. The synthesized Fe_3O_4 was spherical particles with a diameter of ~16 nm. γ-Fe_2O_3 was spherical particles with a diameter of ~12 nm. γ-FeOOH particles were needle-shaped, with a width of ~10 nm and length of ~400 nm.

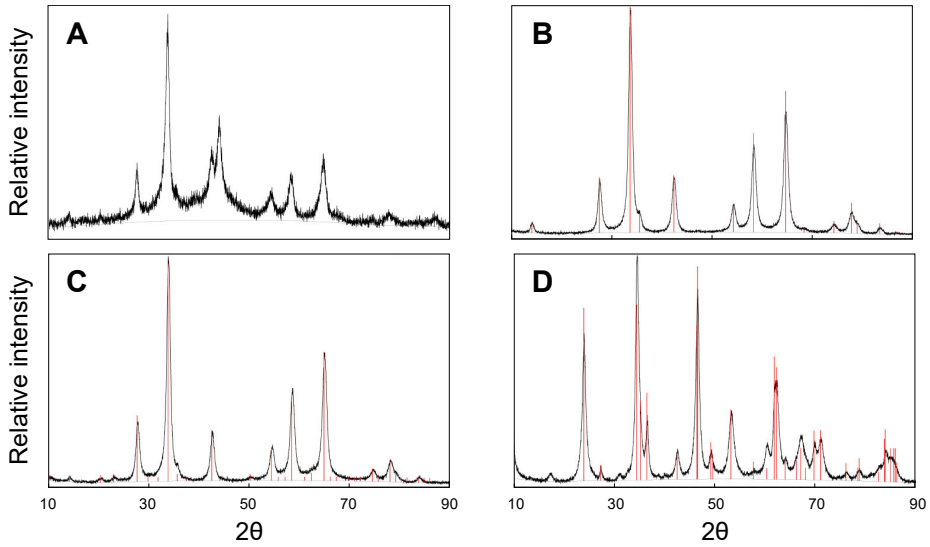

Figure S14. X-ray powder diffraction (XRD) spectra of the (A) aerobically aged nZVI (O-nZVI-72 h); and synthesized (B) Fe_3O_4, (C) γ-Fe_2O_3, and (D) γ-FeOOH compared with standard spectra (red line). The XRD analysis was conducted in ambient air with Cu Kα using a D8 Advance (Bruker) operated at 40 kV and 40 mA. Continuous scans from 10° to 90° at 2θ were collected with a stop size of 0.02° and a count time of 1.0 s per step.

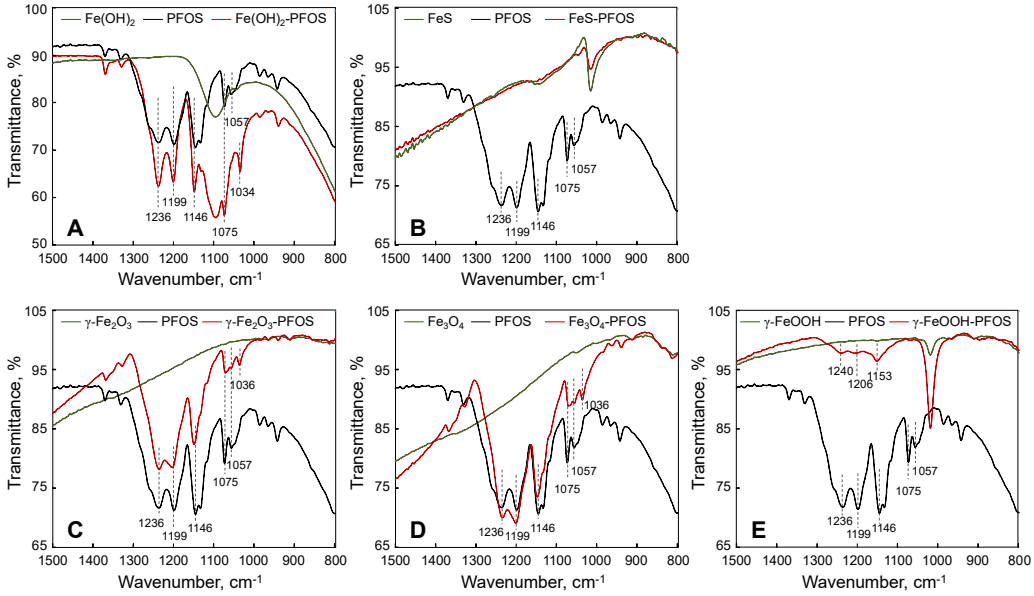

Figure S15. ART-FTIR spectra of PFOS, synthesized iron nanoparticles that represent the iron species formed after aging, and PFOS sorbed on the iron nanoparticles for (A) $Fe(OH)_2$, (B) FeS, (C) γ-Fe_2O_3, (D) Fe_3O_4, and (E) γ-FeOOH. PFOS (500 mg/L) was incubated with 2.0 g/L particles for 5 days before analysis. The peak wavenumbers for characteristic functional groups of PFOS (C–F, R–SO_3^-) are shown.

References

(S1) Arp, H. P. H.; Niederer, C.; Goss, K. U. Predicting the partitioning behavior of various highly fluorinated compounds. *Environ. Sci. Technol.* **2006**, 40 (23), 7298–7304.

(S2) Brooke, D.; Footitt, A.; Nwaogu, T. A. Environmental Risk Evaluation Report: Perfluorooctanesulphonate (PFOS). Wallingford: Environment Agency. 2009.

(S3) Rayne, S.; Forest, K. Theoretical studies on the pK_a values of perfluoroalkyl carboxylic acids. *J. Mol. Struc-THEOCHEM* **2010**, 949 (1), 60–69.

(S4) Parveen, M. F.; Umapathy, S.; Dhanalakshmi, V.; Anbarasan, R. Synthesis and characterizations of nanosized iron (II) hydroxide and iron (II) hydroxide/poly (vinyl alcohol) nanocomposite. *J. Appl. Polym. Sci.* **2010**, 118 (3), 1728–1737.

(S5) Butler, E. C.; Hayes, K. F. Effects of solution composition and pH on the reductive dechlorination of hexachloroethane by iron sulfide. *Environ. Sci. Technol.* **1998**, 32 (9), 1276–1284.

(S6) Rajput, S.; Pittman, C. U.; Mohan, D. Magnetic magnetite (Fe_3O_4) nanoparticle synthesis and applications for lead (Pb^{2+}) and chromium (Cr^{6+}) removal from water. *J Colloid Interf. Sci.* **2016**, 468, 334–346.

(S7) Schwertmann, U.; Cornell, R. M. Iron Oxides in the Laboratory: Preparation and Characterization. John Wiley Sons. **2008**.

(S8) Park, S.; Zenobio, J. E.; Lee, L. S. Perfluorooctane sulfonate (PFOS) removal with Pd^0/nFe^0 nanoparticles: Adsorption or aqueous Fe-complexation, not transformation? *J. Hazard. Mater.* **2018**, 342, 20–28.

(S9) Schwarzenbach, R. P.; Gschwend, P. M.; Imboden, D. M. Environmental Organic Chemistry. Second Ed. Sorption III: Sorption processes involving inorganic surfaces (pp. 287–457). John Wiley Sons, Inc. 2003.

(S10) Xiao, F.; Zhang, X.; Penn, L.; Gulliver, J. S.; Simcik, M. F. Effects of monovalent cations on the competitive sorption of perfluoroalkyl acids by kaolinite: Experimental studies and modeling. *Environ. Sci. Technol.* **2011**, 45 (23), 10028–10035.

(S11) Johnson, R. L.; Anschutz, A. J.; Smolen, J. M. Simcik, M. F.; Penn, R. L. The sorption of perfluorooctane sulfonate onto sand, clay, and iron oxide surfaces. *J. Chem. Eng. Data* **2007**, 52 (4), 1165–1170.

(S12) Tang, C. Y.; Fu, Q. S.; Gao, D.; Criddle, C. S.; Leckie, J. O. Effect of solution chemistry on the sorption of perfluorooctane sulfonate onto mineral surfaces. *Water Res.* **2010**, 44 (8), 2654–2662.

(S13) Lu, X.; Deng, S.; Wang, B.; Huang, J.; Wang, Y.; Yu, G. Adorption behavior and mechanism of perfluorooctane sulfonate on nanosized inorganic oxides. *J. Colloid Interf. Sci.* **2016**, 474, 199–205.

(S14) Wang, F.; Liu, C.; Shih, K. Adsorption behavior of perfluorooctanesulfonate (PFOS) and perfluorooctanoate (PFOA) on boehmite. *Chemosphere* **2012**, 89 (8), 1009–1014.

(S15) Wang, F.; Shih, K. Adsorption of perfluorooctanesulfonate (PFOS) and perfluorooctanoate (PFOA) on alumina: Influence of solution pH and cations. *Water Res.* **2011**, 45 (9), 2925–2930.

(S16) Higgins, C. P.; Luthy, R. G. Sorption of perfluorinated surfactants on sediments. *Environ. Sci. Technol.* **2006**, 40 (23), 7251–7256.

(S17) Pan, G.; Jia, C.; Zhao, D.; You, C.; Chen, H.; Jiang, G. Effect of cationic and anionic surfactants on the sorption and desorption of perfluorooctane sulfonate (PFOS) on natural sediments. *Environ. Pollut.* **2009**, 157 (1), 325–330.

(S18) Guelfo, J. L.; Higgins, C. P. Subsurface transport potential of perfluoroalkyl acids at aqueous film-forming foam (AFFF)-impacted sites. E*nviron. Sci. Technol.* **2013**, 47 (9), 4164–4171.